Bioinspired Assembly of Colloidal Nanoplatelets by Electric Field

Tzung-Hua Lin, Wei-Han Huang, In-Kook Jun, and Peng Jiang*

Department of Chemical Engineering, University of Florida, Gainesville, Florida 32611

Received September 2, 2008. Revised Manuscript Received April 18, 2009

This paper reports a simple electrodeposition technology that enables rapid production of large-area polymer nanocomposites with layered structures that mimic the nacreous layer of mollusk shells. Uniform, electrostatically stabilized gibbsite nanoplatelets with high aspect ratio are preferentially oriented parallel to the electrode surface when an external direct current electric field is applied. The electroplated ceramic films have uniform thickness, and the thickness can be controlled by adjusting the nanoplatelet concentration of the electroplating baths. Homogeneous, optically transparent nanocomposites are obtained when the interstitials between the aligned nanosheets are infiltrated with polymer. The resulting ceramic−polymer nanocomposites exhibit four-times higher tensile strength and nearly 1 order of magnitude higher modulus than pure polymer films. The covalent linkage between the nanoplatelets and the polymer matrix plays an important role in determining the mechanical properties of these biomimetic nanocomposites.

Introduction

Bottom-up self-assembly of nonspherical colloidal building blocks is of great interest for the development of new materials with potential applications in optoelectronics, photonics, magnetics, catalysis, and mechanics.[1−9] Oriented assembly of platelet-like particles is particularly interesting as it enables the production of nanocomposites with greatly improved mechanical properties.[10−12] This is inspired by the ordered assemblies of aragonite (a mineral form of $CaCO_3$) platelets in the nacreous layer of mollusk shells.[13−15] The intricate layered structures consisting of brittle minerals and soft proteins in these natural composites lead to the unique combination of stiffness, strength, and toughness.[1] Mimicking these high-performance layered materials by bottom-up self-assembly has attracted great recent interest.[10,11,16−18] Layer-by-layer (LBL) assembly of ceramic platelets (e.g., nanoclays and alumina) and polymers has been demonstrated to be an efficient methodology in creating reinforced nanocomposites with aligned structures.[11,16] However, LBL assembly is a relative slow process, and hundreds of bilayers need to be deposited to form composites with micrometer-scale thickness. Other bottom-up technologies, such as spin-coating, gravitational sedimentation, and centrifugation, have also been explored to assemble ceramic platelets (mostly clays) into ordered structures.[19−21] Unfortunately, the inevitable agglomeration of clay particles hampers the formation of highly aligned structures and thus impairs the mechanical properties of the resulting composites.

Various synthetic methods have been developed to make fairly monodisperse colloidal platelets with high stability in suspensions.[22−25] For instance, uniform gibbsite ($Al(OH)_3$) nanoplatelets with well-defined hexagon-shape can be synthesized by hydrolysis of $Al(OH_2)_6^{3+}$ at 85 °C.[25,26] The aspect ratio of the synthesized gibbsite nanoplatelets (∼10) is close

* To whom correspondence should be addressed. E-mail: pjiang@che.ufl.edu.

(1) Barthelat, F. *Philos. Trans. R. Soc., A* **2007**, *365*, 2907.
(2) Glotzer, S. C.; Solomon, M. J. *Nat. Mater.* **2007**, *6*, 557.
(3) Hosein, I. D.; Liddell, C. M. *Langmuir* **2007**, *23*, 10479.
(4) Kim, J. W.; Larsen, R. J.; Weitz, D. A. *J. Am. Chem. Soc.* **2006**, *128*, 14374.
(5) Lee, J. A.; Meng, L. L.; Norris, D. J.; Scriven, L. E.; Tsapatsis, M. *Langmuir* **2006**, *22*, 5217.
(6) Lee, J. S.; Lee, Y. J.; Tae, E. L.; Park, Y. S.; Yoon, K. B. *Science* **2003**, *301*, 818.
(7) Love, J. C.; Urbach, A. R.; Prentiss, M. G.; Whitesides, G. M. *J. Am. Chem. Soc.* **2003**, *125*, 12696.
(8) Snyder, C. E.; Yake, A. M.; Feick, J. D.; Velegol, D. *Langmuir* **2005**, *21*, 4813.
(9) Ebina, T.; Mizukami, F. *Adv. Mater.* **2007**, *19*, 2450.
(10) Bonderer, L. J.; Studart, A. R.; Gauckler, L. J. *Science* **2008**, *319*, 1069.
(11) Podsiadlo, P.; Kaushik, A. K.; Arruda, E. M.; Waas, A. M.; Shim, B. S.; Xu, J. D.; Nandivada, H.; Pumplin, B. G.; Lahann, J.; Ramamoorthy, A.; Kotov, N. A. *Science* **2007**, *318*, 80.
(12) Gao, H. J.; Ji, B. H.; Jager, I. L.; Arzt, E.; Fratzl, P. *Proc. Natl. Acad. Sci. U.S.A.* **2003**, *100*, 5597.
(13) Aksay, I. A.; Trau, M.; Manne, S.; Honma, I.; Yao, N.; Zhou, L.; Fenter, P.; Eisenberger, P. M.; Gruner, S. M. *Science* **1996**, *273*, 892.
(14) Jackson, A. P.; Vincent, J. F. V.; Turner, R. M. *Proc. R. Soc. London, Ser. B* **1988**, *234*, 415.
(15) Smith, B. L.; Schaffer, T. E.; Viani, M.; Thompson, J. B.; Frederick, N. A.; Kindt, J.; Belcher, A.; Stucky, G. D.; Morse, D. E.; Hansma, P. K. *Nature* **1999**, *399*, 761.
(16) Podsiadlo, P.; Michel, M.; Lee, J.; Verploegen, E.; Kam, N. W. S.; Ball, V.; Lee, J.; Qi, Y.; Hart, A. J.; Hammond, P. T.; Kotov, N. A. *Nano Lett.* **2008**, *8*, 1762.
(17) Oaki, Y.; Imai, H. *Angew. Chem., Int. Ed.* **2005**, *44*, 6571.
(18) Tang, Z. Y.; Kotov, N. A.; Magonov, S.; Ozturk, B. *Nat. Mater.* **2003**, *2*, 413.
(19) Liu, T.; Chen, B. Q.; Evans, J. R. G. *Bioinspiration Biomimetics* **2008**, *3*, 016005.
(20) Chen, R. F.; Wang, C. A.; Huang, Y.; Le, H. R. *Mater. Sci. Eng., C* **2008**, *28*, 218.
(21) Almqvist, N.; Thomson, N. H.; Smith, B. L.; Stucky, G. D.; Morse, D. E.; Hansma, P. K. *Mater. Sci. Eng., C* **1999**, *7*, 37.
(22) Deng, H.; Yang, S. H.; Xiao, S.; Gong, H. M.; Wang, Q. Q. *J. Am. Chem. Soc.* **2008**, *130*, 2032.
(23) Sun, L. Y.; Boo, W. J.; Sue, H. J.; Clearfield, A. *New J. Chem.* **2007**, *31*, 39.
(24) Kim, H.; Luo, D. W.; Link, D.; Weitz, D. A.; Marquez, M.; Cheng, Z. D. *Appl. Phys. Lett.* **2007**, *91*, 133106.
(25) Wierenga, A. M.; Lenstra, T. A. J.; Philipse, A. P. *Colloids Surf., A* **1998**, *134*, 359.
(26) Wijnhoven, J. *Chem. Mater.* **2004**, *16*, 3821.

10.1021/cm802372f CCC: $40.75
Published on Web 05/01/2009

to that of natural aragonite platelets in nacre.[14] The diameter and thickness of the gibbsite nanoplatelets can be controlled by seeded growth.[27] The gibbsite structure is a stacking of Al−OH layers, and each Al^{3+} is surrounded by six hydroxyl groups. The reaction of surface hydroxyl groups with water makes the nanoplatelets highly charged in water and alcoholic suspensions. The surface hydroxyl groups also facilitate the chemical modification of the particle surface to render different functionalities.[26] By using gibbsite nanoplatelet as a model system, Lekkerkerker et al. have extensively exploited the liquid crystal phase transition in suspensions of plate-like particles.[28−31] Opal-like columnar gibbsite colloidal crystals have also been demonstrated by forced sedimentation.[32,33]

Electrophoresis is a well-established technology in assembling spherical colloids into highly ordered colloidal crystals.[34−36] In this methodology, charged colloids are attracted by electrical force toward the counter electrode and then deposited on the electrode surface by particle coagulation.[37] Electrodeposition is a simple, inexpensive, and scalable technology that enables rapid production of thick films over large areas. Electrophoretic codeposition of colloids and polymer is also possible for the formation of nanocomposites in a single step.[38] In addition, deposition of metals and conducting polymers in the interstitials of colloids is easily achieved by electrophoresis. This will significantly expand the available materials for the fabrication of layered nanocomposites. Electrophoretic assembly of nanoclays has previously been tested, but the entrapment of nonplate particles caused by the agglomeration of nanoclays deteriorates the layered structure.[19]

Here we use electrostatically stabilized gibbsite nanoplatelets with well-defined shape and size as a model system to explore the oriented assembly of plate-like colloids by electrophoresis. A simple spin-coating process has also been developed to infiltrate the interstitials between the assembled nanosheets to form artificial nacreous nanocomposites. The resulting self-standing films are transparent and exhibit significantly improved mechanical properties over those of pure polymer. We can also chemically functionalize the surface of the gibbsite nanoplatelets to facilitate the formation of covalent linkage between the ceramic platelets and the polymer matrix. This further reinforces these biomimetic nanocomposites.

Experimental Section

Materials and Substrates. All solvents and chemicals are of reagent quality and are used without further purification. Ultrapure water (18.2 MΩ cm^{-1}) is used directly from a Barnstead water system. Ethanol (200 proof) is purchased from Pharmaco Products. Hydrochloric acid (37%), aluminum *sec*-butoxide (≥95%), and aluminum isopropoxide (≥98%) are obtained from Aldrich. Ethoxylated trimethylolpropane triacrylate (ETPTA) monomer is provided by Sartomer (Exton, PA). The photoinitiator, Darocur 1173 (2-hydroxy-2-methyl-1-phenyl-1-propanone), is obtained from Ciba Specialty Chemicals. Two-part polydimethylsiloxane (PDMS, Sylgard 184) is provided by Dow Corning. ITO coated glass substrates with sheet resistance of 8 Ω are purchased from Delta Technologies. Silicon wafers (test grade, n type, (100)) are purchased from University Wafer.

Instrumentation. An EG&G Model 273A potentiostat/galvanostat is used for electrophoretic deposition. Scanning electron microscopy (SEM) is carried out on a JEOL 6335F FEG-SEM. A thin layer of gold is sputtered onto the samples prior to imaging. Transmission electron microscopy (TEM) and selected area electron diffraction are performed on a JEOL TEM 2010F. Atomic force microscopy (AFM) is conducted on a Digital Instruments Dimension 3100 unit. X-ray diffraction spectra of the electroplated gibbsite films are obtained with Philips APD-3720 equipment. A Cu $K\alpha_1$ ($\lambda = 1.54049$ Å) radiation is scanned from 10° to 70° with a scan rate of 2.4°/min. Thermogravimetric analysis (TGA) is carried out in air with a Perkin-Elmer thermogravimetric analyzer and a platinum crucible between 20 and 800 °C at a heating rate of 5 °C/min. The zeta potential of gibbsite nanoplatelets is measured by a Brookhaven ZetaPlus Analyzer (Brookhaven Instrument Corporation). An Ocean Optics HR4000 high resolution fiber optic UV−vis−near-IR spectrometer is used for optical transmission measurement. A standard spin-coater (WS-400B-6NPP-Lite spin processor, Laurell) is used to spin-coat ETPTA monomer. The polymerization of ETPTA is carried out on a pulsed UV curing system (RC 742, Xenon).

Synthesis of Gibbsite Nanoplatelets. The gibbsite nanoplatelets are synthesized by following a preparation method as described in ref 25. To 1 L of ultrapure water are added hydrochloric acid (0.09 M), aluminum *sec*-butoxide (0.08 M), and aluminum isopropoxide (0.08 M). The mixture is stirred for 10 days and then heated in a polyethylene bottle in a water bath at 85 °C for 72 h. After cooling to room temperature, dispersions of gibbsite nanoplatelets are centrifuged at 3500*g* for 6 h, and the sediments are redispersed in deionized water. For completely removing the unreacted reactants and concentrating the nanoplatelets, this process is repeated for five times.

Surface Modification of Gibbsite Nanoplatelets. Gibbsite nanoplatelets are surface-modified with 3-(trimethoxysilyl)propyl methacrylate (TPM).[39] Prior to adding gibbsite nanoplatelets, 10 mL of TPM is mixed with 100 mL of a water−methanol solution (water/methanol volume ratio of 3:1) for 1 h to fully hydrolyze TPM. Surface modification is then accomplished by adding 100 mL of gibbsite dispersion (ca. 1 vol % aqueous solution) into the hydrolyzed TPM solution. The suspension is stirred at 40 °C for 30 min. The modified nanoplatelets are washed by repeated centrifugation−redispersion cycles with pure ethanol and finally concentrated to a stock suspension of 0.045 and 0.035 (g/g) in ethanol.

Electrophoretic Deposition. Electrophoretic deposition of gibbsite nanoplatelets is performed in a sandwich cell placed horizon-

(27) Wijnhoven, J. *J. Colloid Interface Sci.* **2005**, *292*, 403.
(28) Mourad, M. C. D.; Wijnhoven, J.; Van 'T Zand, D. D.; Van der Beek, D.; Lekkerkerker, H. N. W. *Philos. Trans. R. Soc., A* **2006**, *364*, 2807.
(29) van der Beek, D.; Lekkerkerker, H. N. W. *Langmuir* **2004**, *20*, 8582.
(30) van der Kooij, F. M.; Kassapidou, K.; Lekkerkerker, H. N. W. *Nature* **2000**, *406*, 868.
(31) van der Kooij, F. M.; Lekkerkerker, H. N. W. *J. Phys. Chem. B* **1998**, *102*, 7829.
(32) van der Beek, D.; Radstake, P. B.; Petukhov, A. V.; Lekkerkerker, H. N. W. *Langmuir* **2007**, *23*, 11343.
(33) Brown, A. B. D.; Clarke, S. M.; Rennie, A. R. *Langmuir* **1998**, *14*, 3129.
(34) Velev, O. D.; Bhatt, K. H. *Soft Matter* **2006**, *2*, 738.
(35) Braun, P. V.; Wiltzius, P. *Nature* **1999**, *402*, 603.
(36) Holgado, M.; Garcia-Santamaria, F.; Blanco, A.; Ibisate, M.; Cintas, A.; Miguez, H.; Serna, C. J.; Molpeceres, C.; Requena, J.; Mifsud, A.; Meseguer, F.; Lopez, C. *Langmuir* **1999**, *15*, 4701.
(37) Zhitomirsky, I. *Adv. Colloid Interface Sci.* **2002**, *97*, 279.
(38) Lin, T. H.; Huang, W. H.; Jun, I. K.; Jiang, P. *Electrochem. Commun.* **2009**, *11*, 14.
(39) Philipse, A. P.; Smits, C.; Vrij, A. *J. Colloid Interface Sci.* **1989**, *129*, 335.

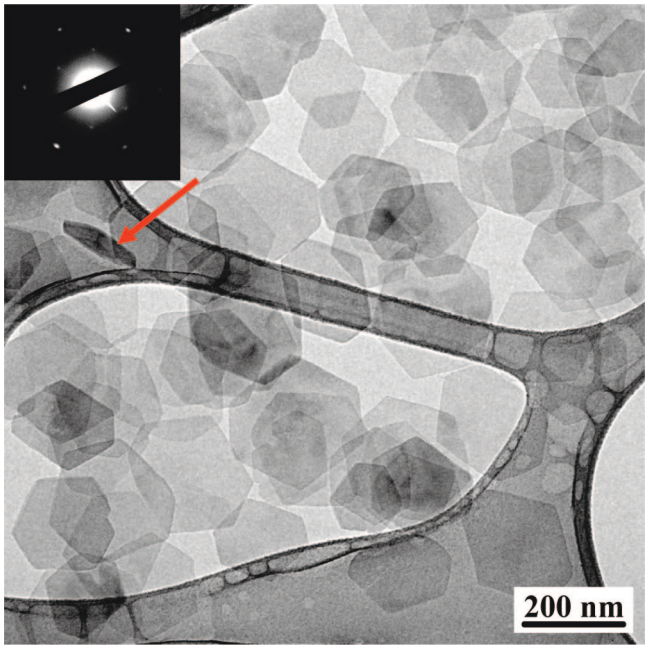

Figure 1. TEM image of gibbsite nanoplatelets. The inset shows the electron diffraction patterns obtained from a single nanoplatelet. The red arrow shows a gibbsite nanoplatelet oriented perpendicularly to the TEM grid.

tally. The bottom and the top of the cell are an ITO working electrode and a gold counter electrode, respectively. The gold electrode is prepared by sputtering deposition of 20 nm of chromium and 200 nm of gold on a (100) silicon wafer. PDMS is used as a spacer to get an active area of 1.5 × 1.5 cm^2 and a cell gap of 2.2 mm. Aqueous suspensions of gibbsite nanoplatelets with different weight percentage are used. Ethanol (200 proof) is added into the suspensions to make the volumetric ratio of ethanol to the aqueous suspension to be 2. A constant voltage of −2.5 V (ITO vs Au) is applied for 30 min to deposit the positively charged gibbsite nanoplatelets onto the ITO cathode. After deposition, the electroplated gibbsite films are rinsed with 200-proof ethanol and then dried with compressed air.

Mechanical Test. For tensile strength measurement, three types of thin films (ETPTA, gibbsite−ETPTA, and TPM-modified gibbsite−ETPTA) are tested using an Instron model 1122 load frame upgraded with an MTS ReNew system and equipped with a 500 g load cell at a crosshead speed of 0.5 mm/min. Testing samples with widths of 1.5 mm and thickness ranging from 30 to 80 μm are adhered on homemade sample holders with a 20 mm gap using polyurethane monomer as an adhesive and then UV-cured. The thickness of the tested samples is measured by cross-sectional SEM to calculate the final tensile strength.

Results and Discussion

Gibbsite nanoplatelets are synthesized from aluminum alkoxides in an acidic aqueous solution at 85 °C.[25] Instead of utilizing a long dialysis process (7−10 days) for purifying the as-made gibbsite nanoplatelets, we use multiple centrifugation−redispersion cycles to remove unreacted agents and small particles. Figure 1 shows a typical TEM image of purified gibbsite nanoplatelets. The particles are hexagonally shaped and are relatively uniform in size. The diameter of the nanoplatelets is measured to be 188 ± 40 nm by averaging over 100 particles from the TEM micrographs. TEM images also reveal that the nanoplatelets tend to align parallel to the surface of TEM grids. It is very rare to find nanoplatelets oriented perpendicularly to the TEM grid surface as shown by the red arrow pointing to such a particle in Figure 1. AFM experiments show the platelet thickness ranges from 10 to 15 nm. The purified gibbsite nanoplatelets are electrostatically stabilized, and the zeta-potential (ζ) of the colloids in deionized water is measured to be +40.5 ± 2.3 mV by fitting experimental data using Smoluchowski's model.[40] The high surface charge makes the nanoplatelets stable in aqueous and alcoholic dispersions, and aggregated particles are rarely seen in TEM images. The selected area electron diffraction (SAED) patterns from a single platelet as shown in the inset of Figure 1 indicate that the as-made gibbsite nanoplatelets are single-crystal.

The electrophoretic deposition of positively charged gibbsite nanoplatelets is carried out using a parallel-plate sandwich cell, which consists of an indium tin oxide (ITO) working electrode, a gold counter electrode, and a polydimethylsiloxane (PDMS) spacer (~2.2 mm thick). The bath solution is gibbsite nanoplatelets dispersed in a water−ethanol mixture with volumetric ratio of 1:2. The volume fraction of gibbsite particles is adjusted to ~1%. Ethanol is added to the aqueous dispersions to reduce the dielectric constant of the solvent and thus reduce the electrical double-layer thickness of the particles to promote colloidal coagulation on the ITO electrode.[37] Without ethanol, no particle deposits are adhered on the working electrode after disassembling the electrical cell. The addition of ethanol also facilitates reduction of cracking and porosity in the electrophoretically deposited films.[37] The applied electric field strength is ~1100 V/m. The electrophoretic velocity of the gibbsite nanoplatelets is estimated to be ~7.5 μm/s by using the Smoluchowski equation: $u_E = (\varepsilon\varepsilon_0\zeta/\mu)E$, where ε is the dielectric constant of the solution, ε_0 is the permittivity of the vacuum, μ is the solution viscosity, and E is the applied electric field strength.[40] For a 2.2 mm thick sandwich cell, the estimated time to deposit most particles on the ITO electrode is about 5 min, agreeing with our experimental observation. Besides parallel-plate geometry, electrodes can also be vertically inserted into the colloidal baths to conduct the electrophoretic deposition. As the gravitational sedimentation of the gibbsite nanoplatelets during the electrophoretic process is negligible, uniform deposits on the electrodes are obtained.

After electrophoretic deposition, the gibbsite deposits on the ITO cathode are washed with ethanol and then dried with compressed air. The deposits can be easily peeled off from the ITO surface by using a sharp razor blade, resulting in the formation of self-standing films as shown in Figure 2A. The film is opaque and brittle, and the side facing the ITO cathode is smoother than the side facing the suspension. The size of the resulting films is solely determined by the dimensions of the ITO electrode. Figure 2A depicts a sample with 1.6 × 0.6 $in.^2$ size deposited on a 2 × 1 $in.^2$ ITO electrode. Figure 2B shows a top-view SEM image of the suspension side of the sample in Figure 2A. The hexagonal gibbsite nanoplatelets are densely packed and aligned parallel

(40) Russel, W. B.; Saville, D. A.; Schowalter, W. R. *Colloidal dispersions*; Cambridge University Press: Cambridge, 1989.

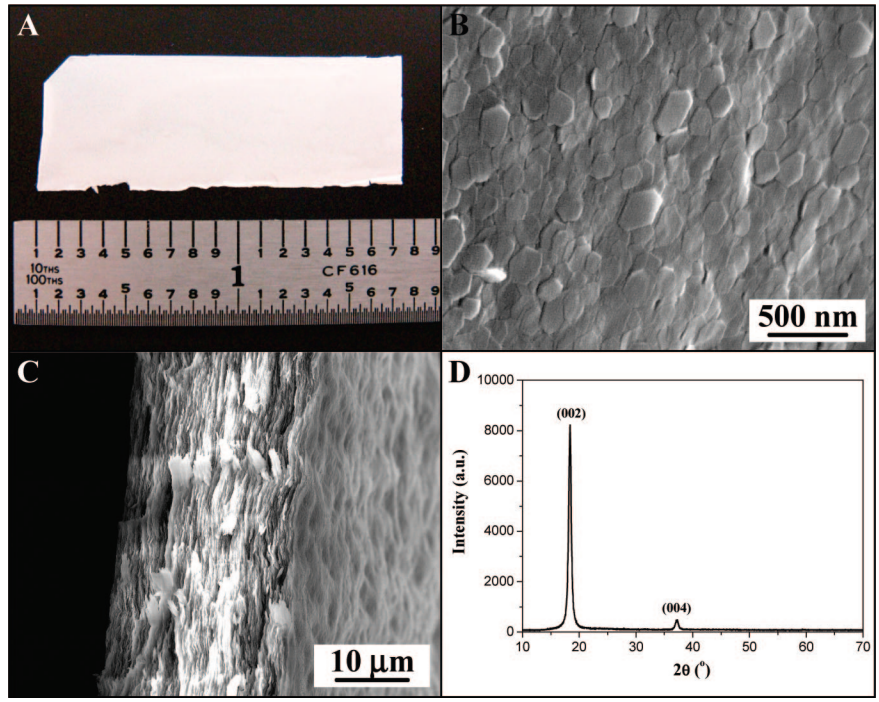

Figure 2. Electrophoretic assembly of gibbsite nanoplatelets. (A) Photograph of a free-standing gibbsite film. (B) Top-view SEM image of the sample in (A). (C) Cross-sectional view of the same sample. (D) XRD patterns of the gibbsite film in (A).

to the electrode surface. The alignment of gibbsite nanoplatelets is further confirmed by the layered structure as shown in the cross-sectional SEM image of Figure 2C. Another convincing evidence of the orientated deposition comes from the X-ray diffraction (XRD) patterns shown in Figure 2D. Only (002) and (004) peaks are observed in the XRD spectrum. As the crystallographic *c*-axis of single-crystal gibbsite is normal to the platelet surfaces, the (002) and (004) reflections are from gibbsite platelets oriented parallel to the electrode surface.[41] Analysis of the half-height width of the (002) peak with the Scherrer equation yields an average platelet thickness of 15.1 nm, agreeing with AFM measurement.

The oriented deposition of gibbsite nanoplatelets in a direct-current (dc) electric field can be understood by considering the charge distribution on the gibbsite surfaces. Early study shows the isoelectric point (IEP) of the edges (pH $\approx$ 7) differs from that on the faces (pH $\approx$ 10).[25] The pH of the suspension in the electrophoretic experiments is close to 7, resulting in positively charged surfaces and almost neutral edges. Therefore, the applied electric field exerts a force only on the surfaces of the gibbsite platelets, and Brownian motion could provide sufficient torque to reorient perpendicular particles to face the ITO electrode. Once close to the electrode, the gibbsite nanoplatelets will be forced to align parallel to the electrode surface as this orientation is more energetically favorable than the perpendicular one. Similar to the evaporation-induced alignment of gibbsite nanoplatelets on TEM grids (Figure 1), further evidence shows that capillary force during solvent evaporation is sufficient to orient gibbsite particles into layered assemblies.

(41) Cullity, B. D. *Elements of x-ray diffraction*, 2nd ed.; Addison-Wesley Publishing Company: Reading, MA, 1978.

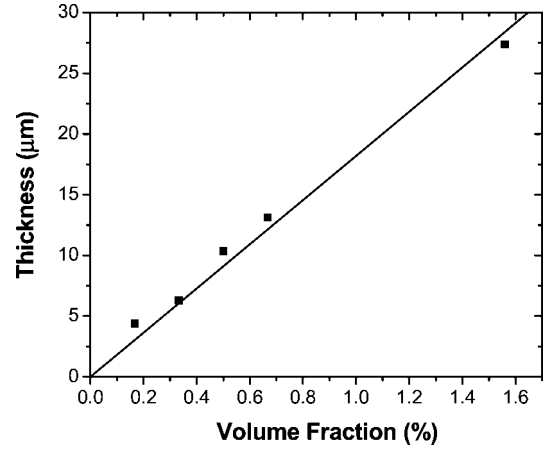

Figure 3. Thickness dependence of the electroplated films on the concentration of colloidal gibbsite suspensions. The thickness standard deviation for all samples is ca. 10%.

However, the rapid and uniform deposition of nanoplatelets over large areas is the major advantage of the electrodeposition technology over evaporation- and gravitational sedimentation-induced assembly.[32,33] If the duration of the electrophoretic process is long enough, almost all gibbsite platelets can be deposited on the ITO electrode. The thickness of the deposits is then linearly proportional to the particle volume fraction of the suspension as shown in Figure 3.

After the oriented assembly, polymer−gibbsite nanocomposites can then be made by filling the interstitials between the aligned nanoplatelets with photocurable monomers, followed by photopolymerization. We chose a nonvolatile monomer, ethoxylated trimethylolpropane triacrylate (ETPTA, M.W. 428, viscosity 60 cps), to form the nanocomposites. The monomer with 1% photoinitiator (Darocur 1173, Ciba-Geigy) is spin-coated at 4000 rpm for 1 min to infiltrate

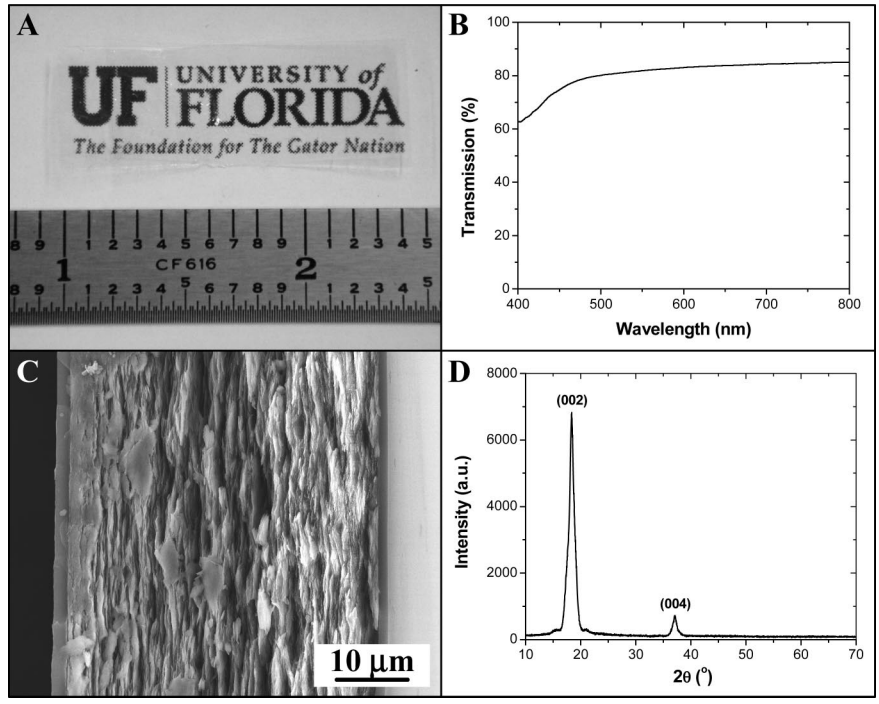

Figure 4. Free-standing gibbsite−ETPTA nanocomposite. (A) Photograph of a transparent film. (B) Normal-incidence transmission spectrum of the sample in (A). (C) Cross-sectional SEM image of the same nanocomposite film. (D) XRD patterns of the nanocomposite sample.

the electroplated gibbsite film and then polymerized by exposure to ultraviolet radiation. The resulting nanocomposite film becomes highly transparent (Figure 4A) as a result of the matching of the refractive index between the gibbsite platelets and the polymer matrix. The normal-incidence transmission measurement as shown in Figure 4B shows that the free-standing nanocomposite film exhibits high transmittance (>80%) for most of the visible wavelengths. As the reflection (R) from an interface between two materials with refractive indices of n_1 and n_2 is governed by Fresnel's equation $R = [(n_1 - n_2)/(n_1 + n_2)]^2$,[42] we can estimate the normal-incidence reflection from each air−nanocomposite interface to be about 4%. Thus, the optical scattering and absorption caused by the nanocomposite itself is approximately 10%. This suggests that the polymer matrix has infiltrated most interstitial spaces between the aligned gibbsite nanoplatelets. The cross-sectional SEM image in Figure 4C shows that the nanocomposite retains the layered structure of the original electroplated gibbsite film, and thin wetting layers of ETPTA (~1 μm thick) are observed on the surfaces of the film. The oriented arrangement of the nanoplatelets is also maintained throughout the polymer infiltration process as confirmed by the distinctive (002) and (004) peaks of the XRD spectrum shown in Figure 4D.

The ceramic weight fraction in the gibbsite−ETPTA nanocomposite film is determined by thermogravimetric analysis (TGA) as shown in Figure 5. From the TGA curve and the corresponding weight loss rate, it is apparent that two thermal degradation processes occur. One happens at ~250 °C and corresponds to the degradation of the polymer matrix, while another occurs at ~350 °C and is due to the decomposition reaction of gibbsite: $2Al(OH)_3 \rightarrow Al_2O_3 + 3H_2O$.[25] On the basis of the residue mass percentage (45.65%) and assuming the ash is solely Al_2O_3, we can estimate the weight fraction of gibbsite nanoplatelets in the original nanocomposite film to be ~0.70. Considering the density of gibbsite (~2.4 g/cm^3) and ETPTA (~1.0 g/cm^3), the volume fraction of gibbsite nanoplatelets in the nanocomposites is approximately 0.50. The complete infiltration of ETPTA between the electroplated gibbsite platelets is further confirmed by the selective dissolution of gibbsite in a 2% hydrochloric acid aqueous solution. This results in the formation of a self-standing porous membrane with stacked hexagon-shaped pores, which are a negative replica of the assembled gibbsite platelets.

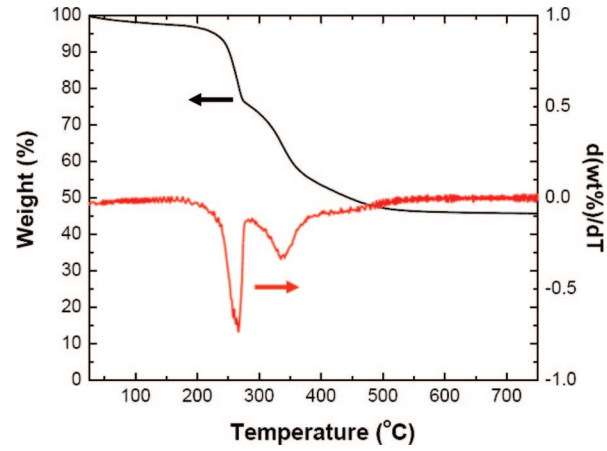

Figure 5. Thermogravimetric analysis of the gibbsite−ETPTA nanocomposite as shown in Figure 4.

The mechanical properties of the biomimetic polymer nanocomposites are evaluated by tensile tests. We compare the tensile strength for three types of thin films, including pure ETPTA, gibbsite−ETPTA, and TPM-modified gibbsite−ETPTA. The surface hydroxyl groups of gibbsite

(42) Macleod, H. A. *Thin-Film Optical Filters*, 3rd ed.; Institute of Physics Publishing: Bristol, 2001.

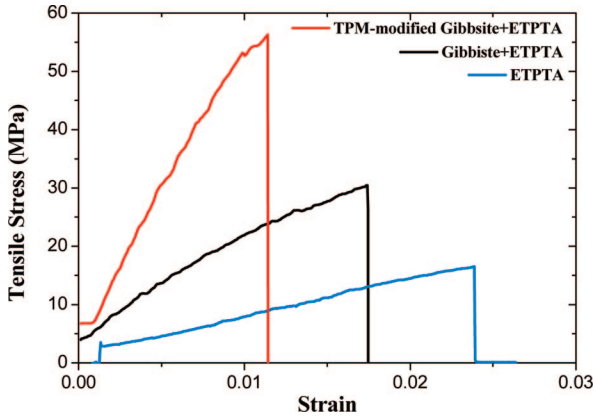

Figure 6. Tensile stress versus strain curves for plain ETPTA film, gibbsite−ETPTA nanocomposite, and TPM-modified gibbsite−ETPTA nanocomposite.

nanoplatelets can be easily modified by reacting with 3-(trimethoxysilyl)propyl methacrylate (TPM) through the well-established silane coupling reaction.[39] This results in the formation of surface-modified particles with dangling acrylate bonds that can be cross-linked with the acrylate-based ETPTA matrix. The colloidal stability and the surface charge of the resulting nanoplatelets are not affected by this surface modification process as confirmed by TEM and zeta potential measurement. Figure 6 shows the tensile stress versus strain curves for the above three types of films. The gibbsite−ETPTA nanocomposite displays ~2 times higher strength and ~3 times higher modulus when compared with pure ETPTA polymer. Even more remarkable improvement occurs when TPM−gibbsite platelets are cross-linked with the ETPTA matrix. We observe ~4 times higher strength and nearly 1 order of magnitude higher modulus than pure polymer. This agrees with early studies that reveal the crucial role played by the covalent linkage between the ceramic fillers and the organic matrix in determining the mechanical properties of the artificial nacreous composites.[11]

We also conduct a simple calculation to evaluate if the measured mechanical properties of the gibbsite−ETPTA nanocomposites are reasonable. For a polymer matrix having a yield shear strength τ_y and strong bonding to the gibbsite nanoplatelet surface (e.g., TPM-modified gibbsites), the tensile strength of the composite (σ_c) can be calculated using the volume fraction of nanoplatelet (V_p), the nanoplatelet aspect ratio (s), and the tensile strength of the nanoplatelet (σ_p) and of the polymer matrix (σ_m), as[10,43]

$$\sigma_c = \alpha V_p \sigma_p + (1 - V_p)\sigma_m \quad (1)$$

For the gibbsite nanoplatelet which has a relatively small aspect ratio ($s \sim 12-18$), the factor α in eq 1 can be estimated as[10,43]

$$\alpha = \frac{\tau_y s}{2\sigma_p} \quad (2)$$

From the above TGA analysis, the volume fraction of gibbsite nanoplatelets in the polymer nanocomposite is ~0.50. If we take $s = 15$, eq 1 can then be simplified as

$$\sigma_c = 3.75\tau_y + 0.5\sigma_m \quad (3)$$

For acrylate-based polymer (like ETPTA), the yield shear strength should be close to its tensile strength. Equation 3 can further be simplified as $\sigma_c \sim 4.25\sigma_m$. This indicates that the strength of the nanocomposite is about fourfold of the strength of the polymer matrix, agreeing with our experimental results (Figure 6).

Conclusions

In conclusion, we have developed a simple and rapid electrodeposition technology for assembling gibbsite nanoplatelets into large-area, self-standing films. These nanosheets with high aspect ratio are preferentially aligned parallel to the electrode surface. The interstitials between the assembled nanoplatelets can be infiltrated with polymer to form optically transparent nanocomposites. The tensile strength and the stiffness of these biomimetic composites are significantly improved when compared to pure polymer films. The current electrodeposition technology is a quite general approach to achieve oriented deposition of platelet-like particles with various aspect ratios. Preliminary results show that silica-coated gibbsite nanoplatelets, hollow silica nanoplatelets, and zeolite platelets can also be aligned by electrophoretic deposition. The technology is also promising for developing layered metal-ceramic and conducting polymer-ceramic nanocomposites that may exhibit improved mechanical and electrical properties but are not easily available by other bottom-up technologies (e.g., LBL assembly).

Acknowledgment. This work was supported in part by the start-up funds from the University of Florida, the UF Research Opportunity Incentive Seed Fund, and the NSF under Grants CBET-0651780 and CBET-0744879.

CM802372F

(43) Glayinchevski, B.; Piggott, J. *J. Mater. Sci.* **1973**, *8*, 1373.